

See discussions, stats, and author profiles for this publication at: <https://www.researchgate.net/publication/26720545>

Morphology and Molecular Mobility of Fibrous Hard alpha-Keratins by H-1, C-13, and Xe-129 NMR

ARTICLE in THE JOURNAL OF PHYSICAL CHEMISTRY B · SEPTEMBER 2009

Impact Factor: 3.3 · DOI: 10.1021/jp904484r · Source: PubMed

CITATIONS

4

READS

38

6 AUTHORS, INCLUDING:



[Maria Baias](#)

New York University Abu Dhabi

26 PUBLICATIONS 285 CITATIONS

[SEE PROFILE](#)



[Crisan Popescu](#)

KAO European Research Laboratory

113 PUBLICATIONS 1,713 CITATIONS

[SEE PROFILE](#)



[Bernhard Bluemich](#)

RWTH Aachen University

306 PUBLICATIONS 4,977 CITATIONS

[SEE PROFILE](#)



[Martin Möller](#)

RWTH Aachen University

640 PUBLICATIONS 14,506 CITATIONS

[SEE PROFILE](#)

Morphology and Molecular Mobility of Fibrous Hard α -Keratins by ^1H , ^{13}C , and ^{129}Xe NMR

Maria Baias,[†] Dan E. Demco,^{*,‡,§} Daniel Istrate,[‡] Crisan Popescu,^{*,‡,||} Bernhard Blümich,[†] and Martin Möller[‡]

DWI an der RWTH Aachen, Pauwelsstrasse 8, D-52056 Aachen, Germany, Institut für Technische und Makromolekulare Chemie, RWTH Aachen University, Worringer Weg 1, D-52074 Aachen, Germany, Technical University Cluj-Napoca, Department of Physics, RO-400020 Cluj-Napoca, Romania, and University “Aurel Vlaicu” Arad, Bd. Revolutiei 77, RO-310130 Arad, Romania

Received: May 14, 2009; Revised Manuscript Received: July 14, 2009

The morphology and molecular mobility changes of the side chains for hard α -keratin due to oxidative and reductive/oxidative treatments for temperatures around the DSC denaturation peak were investigated by ^1H , ^{13}C , and ^{129}Xe NMR spectroscopy and ^1H spin diffusion. Proton wide-line spectra were used to obtain the phase composition (rigid, interface, and amorphous fractions) and molecular dynamics of each phase. Proton spin diffusion experiments using a double-quantum filter and initial rate approximation were employed to obtain the dependence of the rigid domain sizes on chemical treatments and denaturation temperatures. A drastic reduction in the rigid domain thickness takes place for the reductive/oxidative treatment. The keratin mobility gradient in the interfacial region at different denaturation temperatures was measured for hard α -keratin from ^1H spin diffusion data. ^{13}C CPMAS spectra were used to provide a detailed examination of the effects of the chemical treatments especially on the disulfide bonds. Thermally polarized ^{129}Xe spectra suggest the existence of voids in the hard α -keratin induced by the reductive and oxidative treatment. The surface of the hard α -keratin fiber surface is probed by the laser hyperpolarized ^{129}Xe . A qualitative model describing the changes induced in hard α -keratin protein by chemical transformation was developed and could be correlated with the changes in domain thickness, phase composition, and molecular dynamics.

1. Introduction

The hard α -keratin is a filament protein found in mammalian epidermal appendages (hairs, quills, horn, nails, etc.) distinct from feather β -keratin found in avian and reptilian tissues. The hair is the most sophisticated biological composite material.¹ The structure of hard α -keratin is characterized by three structural hierarchy levels.² At high resolution, the intermediate filament (IF) protein is made of a central rod domain of amino acid sequences (1A, 1B, 2A, and 2B) containing an aminoacid heptad repeat unit, and separated by loop links (L1, L12, and L2).^{3,4} At the extremity of the rod domain are located the globular C- and N-terminal domains arranged mostly in β -sheets and formed of sulfur rich compounds.^{5,6} Two strands of α -helices are coiled coil to form a superhelical dimer. At the medium resolution, i.e., the intermediate level arrangement of the heterodimers inside IFs, the molecules are assembled both longitudinally and laterally in an ensemble called a microfibril.⁷ The dimers are associated as tetramers, which group to form a long cylinder-shaped intermediate filament with 32 keratin chains in cross section. At lower structural resolution, the bundles of parallel IFs are organized in an amorphous and disordered crystalline lateral network. These are embedded in a sulfur-rich protein matrix of intermediate filament associated proteins (IFAPs) and form a macrofibril, the main morphological component of hard α -keratin fibers.^{1,2}

Although the above model was proposed for describing the mechanic behavior of keratins, it appeared to also be suitable for explaining the high denaturation temperature found in keratins.^{8,9} In soluble proteins, the helix denaturates (unfolds) at temperatures up to 80 °C. There are no data on the denaturation temperature of IFs alone (not surrounded by a matrix), but one may expect that the α -helix from keratins would also unfold at temperatures around 80 °C. It is assumed that the fact that keratin proteins show denaturation at above 100 °C is due to the rigidity of the matrix, whose viscosity impedes the unfolding of the helix. The viscosity (and cross-link) of the matrix governs, therefore, the segmental mobility of the α -helix and the unfolding reaction (denaturation).

A similar model was proposed for collagen based materials.¹⁰ The model suggests that adding solvents able to decrease the viscosity of the matrix depresses the temperature of unfolding. This has been indeed noticed in differential scanning calorimetry (DSC) experiments with keratin fibers^{11,12} and with collagen based materials (parchments, leathers) in a water environment.^{13–15} Understanding properly how the keratins protect the intermediate filaments against thermal denaturation until high values of temperature is of a clear interest for the fundamental knowledge of protein denaturation. The role of the matrix in this process may suggest ways for designing high-temperature stable proteins as new biomaterials.

Multinuclear and multidimensional liquid- and solid-state NMR are important techniques in structural biology.^{16–18} Recently, a ^{13}C and ^2H solid-state NMR study of an α -keratin sourced from equine hoof has revealed a strong dependence of molecular conformation and molecular dynamics on the degree of hydration of the material.¹⁹ In particular, dehydration results

* Corresponding authors. Fax: +49-241-233-01. E-mail: demco@mc.rwth-aachen.de (D.E.D.); cpopescu@dwi.rwth-aachen.de (C.P.).

[†] RWTH Aachen University.

[‡] DWI an der RWTH Aachen.

[§] Technical University Cluj-Napoca.

^{||} University “Aurel Vlaicu” Arad.

in a much more rigid and ordered structure, with a loss of α -helical components in the structure and breaking of cysteine disulfide bonds. Moreover, the molecular dynamics and structural organization of mouse epidermal keratin intermediate filaments (IFs) have been studied via ^{13}C and ^2H spectroscopy and relaxometry on IFs labeled with isotopically enriched amino acids.²⁰ Solid-state ^{31}P NMR spectroscopy was also applied to the analysis of phosphorylated wool keratin to investigate the changes induced on the surface of wool keratin.²¹

The clarification of the fine structure of fibrous proteins like keratin in the solid state is important for the understanding of their nature. This may be achieved because ^{13}C and ^{15}N chemical shifts of polypeptides are substantially dependent on their main-chain conformations such as α -helix and β -sheet forms. Using this method, it was confirmed that both right-handed α -helix and β -sheet forms exist in native wool fiber.^{22–24}

Spin diffusion NMR was proved to be a useful method for characterization of semicrystalline polymer morphology.^{25–29} The sizes of the rigid, interfacial, and amorphous fractions can be estimated from such experiments and the results compared well to that from TEM and X-ray diffraction. Recently, the morphological domain sizes of thermally denatured wool keratin were measured by ^1H spin diffusion NMR experiments.³⁰ For the interpretation of these experiments, the solutions of the spin diffusion equations for two-dimensional square and cylindrical morphologies were employed. The keratin mobility gradient in the interfacial region at different denaturation temperatures was also measured from the ^1H spin diffusion data. A qualitative model describing the denaturation process of hydrated keratin protein was developed that explains the changes in domain thickness, spin diffusivities, phase composition, and thermodynamic parameters.

The aim of this work is to investigate the changes induced by various chemical treatments on hair keratin and the thermal denaturation process of these materials by ^1H NMR wide-line spectroscopy and ^1H spin diffusion. Moreover, cross-polarization magic angle spinning (CPMAS) ^{13}C NMR spectra and thermally polarized and hyperpolarized ^{129}Xe spectra were used for this purpose. The phase (fraction) composition is measured from ^1H wide-line spectra *ex situ* for native and chemically treated Caucasian hair sampled at different temperatures during the denaturation process. Three fractions are detected, i.e., rigid, interfacial, and amorphous. The rigid domain sizes for the hair samples were measured by ^1H spin diffusion using initial-rate approximation. The molecular dynamics gradient of the interfacial region was investigated using the ^1H spin diffusion NMR experiments. The changes in the degree of fibrous hard α -keratin organization, the amount of different phases, and molecular dynamics are discussed in correlation with the type of hair chemical treatments and temperatures during the thermal denaturation process.

2. Experimental Section

2.1. Samples. The hard α -keratin fibers used for this study were of Caucasian dark-brown hair, supplied by Kerling International Haarfabrik GmbH, Germany. The fibers were cleaned with 1% lauryl ether sulfate (LES) and dried at room temperature prior to working with them. The pH of their aqueous extract was found to be 6.5–7.

The damage of the keratin fibers was induced by oxidative and reductive/oxidative chemical treatments, respectively.

The oxidative treatment was performed on 1 g of keratin fibers with 0.2 g of potassium persulphate mixed with 1.2 mL of 6% hydrogen peroxide solution to form a paste adjusted at pH 8.5–9

with ammonia. The fibers were covered with the paste, massaged gently between the fingers, and left 30 min to react at room temperature. The fibers were then rinsed thoroughly until the pH of the aqueous extract was checked to be 7. The treatment was resumed two more times.

The reductive/oxidative treatment was performed with thioglycolic acid (TGA) and hydrogen peroxide. A 1 g portion of keratin fibers, pretreated with water, was immersed for 30 s in the reducing solution of 8% w/w TGA at pH 8.5–9 adjusted with ammonia, the solution excess being removed by gently pressing the fibers between the fingers, then covered with plastic folia and let to react for 30 min at room temperature. The fibers were then rinsed with tap water (3 min) and immersed in the oxidative (hydrogen peroxide 3%) solution adjusted at pH 4.5 with phosphoric acid, for 30 s. After squeezing between fingers, fibers were allowed to react with the oxidative solution for 10 min, at room temperature. Finally, the fibers were washed thoroughly under tap water for 3 min, shampooed for 1 min (70% Natrium Laurethsulfat, pH 7), rinsed with warm water for 1 min, rinsed with tap water for 3 min, and dried under hot air blow. The process was repeated two more times.

Separately, we have prepared a sample in which the disulfide bonds were broken and protected by alkylation. A 1 g portion of fibers was reacted with 8 mL of 0.5 M tris(2-carboxyethyl)phosphine hydrochloride (TCEP), at pH 7 adjusted with ammonium hydroxide, 48 h under continuous stirring at room temperature. After removing the TCEP solution excess, 10 mL of iodacetamide (1 M, pH 8) was added without previously washing the fiber material (to avoid reformation of disulfide bonds) and the sample was kept for 48 h under continuous stirring at room temperature and in the dark. Eventually, the fibers were rinsed under tap water for 3 min, two times subsequently washed with a solution of Texapon N70, 0.1 mL/L (70% sodium laurethsulfat), rinsed again with warm water for 1 min and then tap water for 3 min, and dried in air.

2.2. DSC Measurements. The DSC experiments were run in a DSC-7 Perkin-Elmer instrument calibrated with indium and palmitic acid, both of high purity, using pressure resistant stainless steel large volume capsules. DSC calibration was done with indium and palmitic acid, both of high purity. We used a heating rate of 10 K/min for temperatures ranging from 60 to 180 °C. Each experiment was repeated three to five times, for ensuring the reproducibility of data.

Prior to the DSC measurements, the samples were cut into fine snippets (about 2 mm) and stored under controlled conditions (about 24 h at 22 °C and 55% relative humidity) to ensure invariant water contents. The amount of 7–10 mg of each sample snippets were weighted and placed in crucible for the DSC measurements. Prior to sealing a crucible, 50 μL of distilled water (pH 6.7) was added, and the sealed crucible was stored overnight for about 14 h, to allow the fibers to wet. The samples for NMR measurements were gathered from DSC experiments by taking the pans at various moments linked to thermal events as disclosed by DSC. Three different samples, which will be reported below, were collected this way at various temperatures including the denaturation temperature.

2.3. Proton and ^{13}C NMR Measurements. Proton solid-state NMR spectra, ^1H double-quantum (DQ) build-up curves, ^1H spin diffusion, and ^{13}C CPMAS spectra were measured on a Bruker DSX-500 spectrometer operating at 500.45 and 125.84 MHz for ^1H and ^{13}C , respectively. Proton NMR data were collected at room temperature for nonspinning samples. The dead time of the spectrometer is 5.5 μs . The length of a $\pi/2$

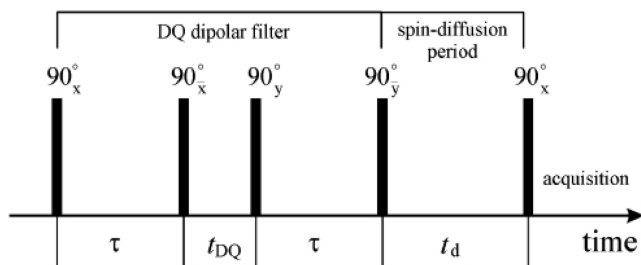


Figure 1. Scheme for the spin diffusion experiment with a DQ filter. The first two pulses excite DQ coherences that evolve for a short time t_{DQ} . These coherences are converted by the following two pulses into z -magnetization. The spin diffusion takes place during the time interval of duration t_d . The last pulse readout is the distribution of magnetization between different keratin phases.

pulse was about $5.5 \mu\text{s}$, the dwell time was $2 \mu\text{s}$, and the recycle delay was 3 s for all measurements.

Proton spin diffusion measurements were performed using the general scheme consisting of a double-quantum (DQ) dipolar filter, a spin diffusion period, and an acquisition period, as presented in Figure 1. The gradient of magnetization was created by the dipolar filter that excites DQ coherences (Figure 1) and selects mainly the magnetization of the rigid phase (fraction).^{28–30} The pulse sequence is based on the two pulses acting during the excitation and reconversion periods. The value of the excitation/reconversion times used in the spin diffusion experiments is $\tau = 7 \mu\text{s}$. It corresponds to the rising region of the DQ build-up curve for each sample (see below).

The experimental wide-line spectra were decomposed into three components using the DMFIT program. The broad component describing the rigid fraction of the spectra was approximated by a Gaussian function. A Lorentzian line shape was used to describe the narrow component of the spectra corresponding to the mobile phase. A combination of Gaussian and Lorentzian functions was used to describe the intermediate line corresponding to the interface.

The proton NMR DQ build-up curves were recorded for setting the optimum parameters of the DQ dipolar filter. They were measured on a Bruker DSX-500 spectrometer at a proton resonance frequency of 500.45 MHz . The duration of the applied 90° pulses was $5.5 \mu\text{s}$. The DQ evolution time and the z -filter delay were fixed to $t_{\text{DQ}} = t_d = 5 \mu\text{s}$ (Figure 1).

^{13}C NMR spectra were measured using cross-polarization (CP) magic-angle sample spinning (MAS) with power decoupling by the two-pulse phase modulation (TPPM) method at a rotor frequency of 5 kHz . The contact pulse for CP has a duration of 2 ms . All NMR measurements were made at room temperature.

2.4. Hyperpolarized and Thermally Polarized ^{129}Xe NMR Measurements. The Rb–Xe gas hyperpolarizer working in the continuous flow mode was built at the Research Centre Jülich, Germany, by the group of S. Appelt. The gas mixture used for hyperpolarization consists of 98% helium, 1% nitrogen, and 1% xenon at a pressure of 7 bar. The gas flow through the pumping cell and the flow can be regulated by a needle valve and controlled by a flowmeter. The typical flow rate used was about $300 \text{ cm}^3/\text{min}$. The total degree of polarization which was achieved by this hyperpolarizer varied in the range 20–35%. The xenon pressure was 5 bar during the NMR measurements. The hyperpolarized ^{129}Xe gas flows through a 7 m plastic tube into the sample cell which is positioned in a 200 MHz Bruker spectrometer. During the transit time to the fringe field of the NMR spectrometer, the hyperpolarized ^{129}Xe gas experienced

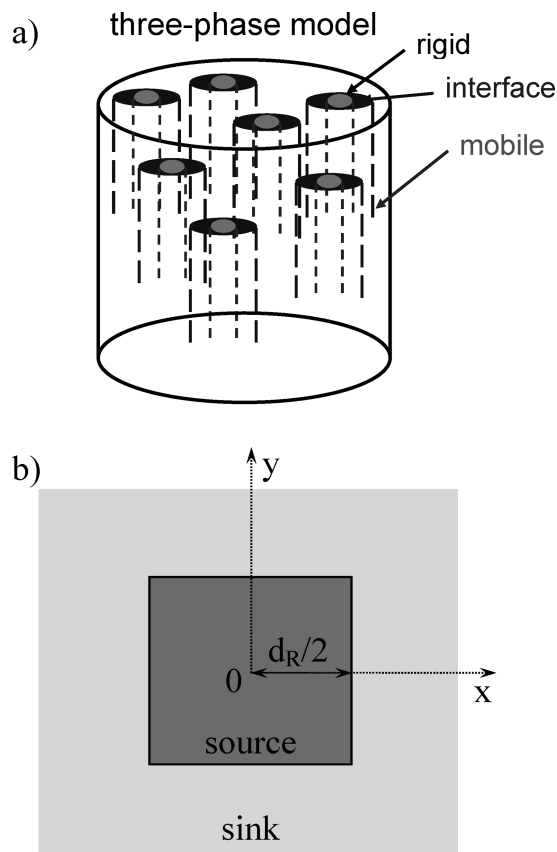


Figure 2. (a) Schematic representation of the three-phase model of keratin fibers. The intermediate filaments (IFs) are imbedded in an amorphous keratin matrix and stabilized by the interface. (b) Schematic representation of the square morphologies with finite source and semi-infinite sink used to approximate the initial regime of the spin diffusion process. The size of the rigid domain is dotted by d_R .

the stray magnetic field of the superconductive magnet. Due to the short transit time of about 50 s , the depolarization was assumed to be negligible.

The ^{129}Xe NMR spectra were measured at a resonance frequency of 55.3 MHz and room temperature. The length of the radio frequency pulse was $50 \mu\text{s}$, and the recycle delay was 30 s . The partial dehydration of the hair samples was obtained by keeping the samples for several hours under a vacuum until the pressure in the system reached $6 \times 10^{-4} \text{ mm Hg}$.

The NMR spectra measured with thermally polarized ^{129}Xe used a homemade sapphire tube with a volume of 4.89 cm^3 sealed by a titanium valve which was approved for pressures up to 50 bar. For the NMR measurements, the tube was loaded with ^{129}Xe gas at a natural abundance of 26.4% and a pressure of 20 bar. The ^{129}Xe NMR spectra were measured at room temperature with a Bruker 500 MHz NMR spectrometer with a recycle delay of 120 s .

3. Theory of NMR Spin Diffusion

3.1. Spin Diffusion Observables. The transport of z -magnetization oriented along the static magnetic field in an NMR experiment can be described by the diffusion equation in the continuum approximation. The concentration $m(\vec{r}, t)$ of nuclear z -magnetization at the position \vec{r} in the sample from the center of symmetry of different morphologies (cf. Figure 2) at the moment of time t is defined by

$$m(\vec{r}, t) = \frac{M_z(\vec{r}, t)}{\rho(\vec{r})\Delta V(\vec{r})} \quad (1)$$

where $M_z(\vec{r}, t)$ is the total z -magnetization and $\Delta V(\vec{r})$ is the infinitesimal volume around the point defined by the vector \vec{r} . The number density of spins is denoted by $\rho(\vec{r})$.

In the limit of isotropic spin diffusion and spatially constant spin diffusivity (D), the spin diffusion equation has the form

$$\frac{\partial m(\vec{r}, t)}{\partial t} = D\nabla^2 m(\vec{r}, t) \quad (2)$$

The instantaneous NMR observables in a spin diffusion experiment are represented by the normalized integral intensity $I_i(t)/I_0$ of the i th component of the NMR spectrum with the total integral intensity I_0 . More specific, the NMR spin diffusion observables are defined by

$$\frac{I_i(t)}{I_0} = \frac{\iiint_{V_i} \rho_i m_i(\vec{r}, t) d\vec{r}}{I_0} \quad (3)$$

where V_i is the volume of the i th domain.

3.2. Solution of the Spin Diffusion Equation for a Finite Source and Semi-Infinite Sink. The real morphology of keratin in hair can be approximated by a square transverse morphology (Figure 2). We assume that the spin diffusion takes place in a heterogeneous matrix from a source R with low segmental mobility represented by the intermediate filaments into a semi-infinite sink M with larger segmental mobility corresponding to the amorphous phase of the keratin. The above morphology is valid only for short spin diffusion times t , i.e., $t < d_R^2/D_R$, where d_R is the size of the rigid domain R (source of magnetization) and D_R is the spin diffusivity for the R domain. The interfacial region is taken together with the amorphous fraction in the following considerations.

The solution of the spin diffusion equation for the composite medium of finite source and semi-infinite sink can be obtained using the solution for a one-dimensional (1D) composite medium.^{27,31–33} For an ε -dimensional diffusion process with $\varepsilon > 1$, the solution of the spin diffusion equation can be written simply as a product of the solutions for the 1D diffusion process.²⁷ For this, the essential condition is that the initial conditions must be expressible as a product of those for the one-variable problems taken separately. The space and time evolution of the concentration of magnetization in the R domain is given by²⁷

$$m_R(\vec{r}, t) = \frac{\rho_R\sqrt{D_R}m_{R0} + \rho_M\sqrt{D_M}m_{M0}}{\rho_R\sqrt{D_R} + \rho_M\sqrt{D_M}} - \frac{\rho_M\sqrt{D_M}(m_{M0} - m_{R0})}{\rho_R\sqrt{D_R} + \rho_M\sqrt{D_M}} \prod_{i=1}^{\varepsilon} \text{erf}\left\{\frac{d_R/2 - x_i}{\sqrt{4D_R t}}\right\} \quad (4)$$

where x_i are the coordinates of the vector $\vec{r}(x_1, x_2, x_3)$ and $x_i < d_R/2$. The error function is defined as

$$\text{erf}(z) = \frac{2}{\sqrt{\pi}} \int_0^z e^{-x^2} dx \quad (5)$$

A highly efficient dipolar filter is characterized by the initial concentration of magnetization: $m_{R0} \neq 0$ and $m_{M0} = 0$. For such a condition, eq 4 has the form

$$m_R(\vec{r}, t) = \frac{\rho_R\sqrt{D_R}m_{R0}}{\rho_R\sqrt{D_R} + \rho_M\sqrt{D_M}} + \frac{\rho_M\sqrt{D_M}m_{R0}}{\rho_R\sqrt{D_R} + \rho_M\sqrt{D_M}} \times \prod_{i=1}^{\varepsilon} \text{erf}\left\{\frac{d_R/2 - x_i}{\sqrt{4D_R t}}\right\} \quad (6)$$

Using the results presented in ref 27 (eq 30) and the above eqs 3, 5, and 6, we get for the time evolution of the integral intensity of the NMR signal from domain R the relationship

$$\frac{I_R(t)}{I_0} = \frac{\rho_R\sqrt{D_R}}{\rho_R\sqrt{D_R} + \rho_M\sqrt{D_M}} + \frac{\rho_M\sqrt{D_M}}{\rho_R\sqrt{D_R} + \rho_M\sqrt{D_M}} \times \left\{1 - \frac{4\sqrt{D_R t}}{d_R} \left[\frac{1}{\sqrt{\pi}} - \text{i erf}c\left(\frac{d_R}{4\sqrt{D_R t}}\right) \right]\right\}^{\varepsilon} \quad (7)$$

where the integral error complement function is

$$\text{i erf}c(z) = \int_z^\infty (1 - \text{erf}(x)) dx \quad (8)$$

At the beginning of the spin diffusion process for short spin diffusion times t , the quantity $d_R/(D_R t)^{1/2} \gg 1$ and $\text{i erf}c(\infty) = 0$. It is evident from eq 7 that, in the initial regime of the spin diffusion, i.e., for $t \ll d_R^2/D_R$, the time dependence of the NMR observable $I_R(t)/I_0$ is linear in $(t)^{1/2}$ and is given by

$$\frac{I_R(t)}{I_0} \approx \frac{\rho_R\sqrt{D_R}}{\rho_R\sqrt{D_R} + \rho_M\sqrt{D_M}} + \frac{\rho_M\sqrt{D_M}}{\rho_R\sqrt{D_R} + \rho_M\sqrt{D_M}} \times \left\{1 - \frac{4\varepsilon\sqrt{D_R t}}{\sqrt{\pi}d_R}\right\} \quad (9)$$

The spin diffusion decay curve described by eq 9 corresponds to an initial slope straight line that intersects the $(t)^{1/2}$ axis at $(t_0)^{1/2}$. The domain thickness d_R for a rectangular 1D, 2D, or 3D morphology is given from eq 9 by

$$d_R \approx \frac{4\varepsilon}{\sqrt{\pi}} \frac{\rho_M\sqrt{D_R D_M}}{\rho_R\sqrt{D_R} + \rho_M\sqrt{D_M}} \sqrt{t_0} \quad (10)$$

In the time regime in which the spin diffusion is not affected by the spin-lattice relaxation, the theorem of total magnetization conservation leads to

$$\frac{I_R(t)}{I_0} + \frac{I_M(t)}{I_0} = 1 \quad (11)$$

Hence, from eqs 9 and 11, the time evolution of the spin diffusion build-up curve for the sink domain (M) has the same slope as that of the source domain. The intercept of the tangent straight line starting from $t = 0$ with the horizontal line at $I(0)/$

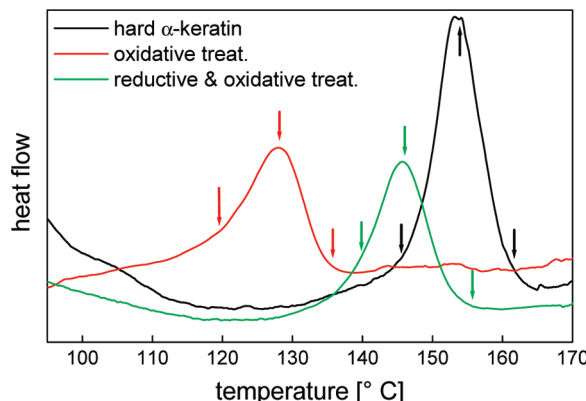


Figure 3. DSC signals of hard α -keratin, in the native state and after oxidative and reductive/oxidative treatments in D_2O for the denaturation temperatures. The arrows mark the temperatures at which the samples were used in the NMR measurements.

$I_0 = 1$ for the spin diffusion build-up curve will lead to the same t_0 value as that of the decay curve eq 10. This is a direct consequence of finite and semi-infinite morphology. This morphology is a good approximation for the morphology with both finite domains in the initial-rate regime. The thickness of the mobile domain d_M can be obtained by the same procedure discussed above using a Goldman–Shen dipolar filter.³⁴

We can also note that the derivation of the relationship for d_R (eq 10) employs only the solution of the spin diffusion equation with corresponding initial and boundary conditions. Moreover, the time evolution is considered for the normalized magnetization. This is not the case for the intercept spin diffusion time reported in refs 26 and 35 where the phase structure considerations and magnetization at equilibrium were taken into account.

4. Results and Discussion

4.1. Thermal Denaturation by DSC. Typical DSC plots in D_2O for the temperature range of denaturation of hard α -keratin in the untreated state, after oxidative, and after reductive and oxidative treatment, respectively, are shown in Figure 3. The endothermal process recorded around 154 °C for the untreated sample is attributed to the thermal denaturation of keratin by melting of the α -helix crystalline structure.²⁶ The scenario for the thermal denaturation of hard α -keratin in the native state and after chemical treatments as reflected in the DSC and NMR data will be discussed below.

4.2. Proton NMR Spectra, Phase Composition, and Molecular Dynamics. The proton NMR spectrum of hard α -keratin, recorded under static conditions at room temperature, is presented in Figure 4. The best fitting parameters have been found by decomposing the spectra in three lines described by a Gaussian, a Lorenzian, and a combination of Gaussian and Lorenzian functions, respectively. The broad component, associated with the Gaussian line, corresponds to the rigid phase. The Lorenzian line associated with the narrow component of the spectra describes the mobile phase. The intermediate line, described by the combination of Gaussian and Lorenzian functions, is associated with the interface.

The phase composition for hard α -keratin, in the native state and after oxidative and reductive/oxidative treatments in D_2O for the temperature range where denaturation takes place is shown in Figure 5. The denaturation temperature of hard α -keratin is 154 °C, that for the hair samples after the oxidative treatment is 122 °C, and that for the sample subjected to

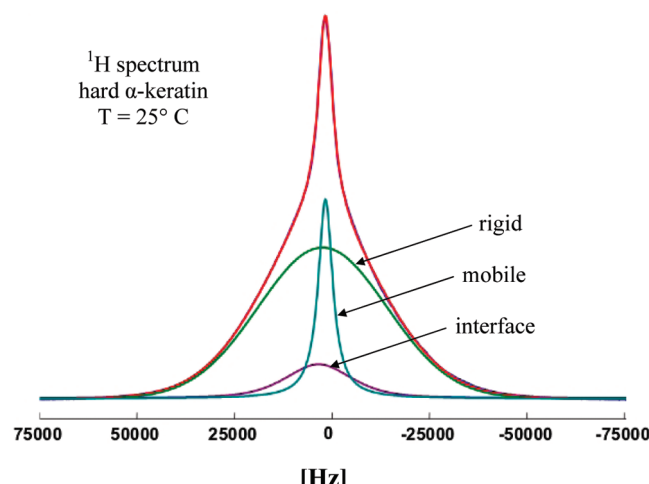


Figure 4. Proton wide-line NMR spectrum of hard α -keratin. All NMR spectra were decomposed into three components corresponding to the rigid, semirigid (interface), and mobile fractions.

reductive/oxidative treatment is 144 °C. The measurements reveal a slight increase in the relative amount of rigid phase and a decrease of the interface for native hard α -keratin. We can note an opposite behavior for the sample after the oxidative and reductive/oxidative treatments. The amount of mobile (amorphous) fraction is not essentially affected by the denaturation temperature. The reductive/oxidative treatment increases the relative amount of rigid fraction as the expense of interface compared to the hard α -keratin.

The molecular dynamics of hard α -keratin, after oxidative and reductive and oxidative treatments for the temperature range where denaturation occurs reflected in the line width of the 1H spectral components is shown for the rigid, interface, and mobile fractions in Figure 6. In general, denaturation at 180 °C induces a greater disorganization in the nanostructured keratin and hence a large molecular mobility. An exception is the mobile fraction of the sample after reductive/oxidative treatment. The molecular motion is strongly hindered by the matrix disorganization induced by this chemical treatment. The molecular motions are more hindered for the rigid phase and interface of hard α -keratin.

4.3. Double-Quantum Dipolar Filter for 1H Spin Diffusion. The spin diffusion experiments observe the equilibration of spatially heterogeneous magnetization over the sample. A magnetization gradient can be created, for example, with a dipolar filter which excites double-quantum (DQ) coherences.²⁴ This type of filter is more advantageous than a dipolar filter for mobile domains because it allows a more accurate detection of the narrow signals on the top of the broad component as compared to the detection of a broad component under a narrow signal. This is valid especially at short diffusion times when the magnetization of one of the components is very small.

The DQ filter can be set such to select the magnetization only from the most rigid part of a heterogeneous sample. By choosing appropriate excitation/reconversion times τ (Figure 1) of the double-quantum coherences, the magnetization corresponding to the stronger dipolar couplings will pass through the filter and that of the weaker dipolar couplings is filtered out. The optimum value of τ can be chosen by recording 1H DQ build-up curves. The maxima of the DQ build-up curves appear at very short excitation/reconversion times τ of about 10–12 μs for all investigated samples. In this range of τ values, the mobile component is completely filtered out, as shown below.

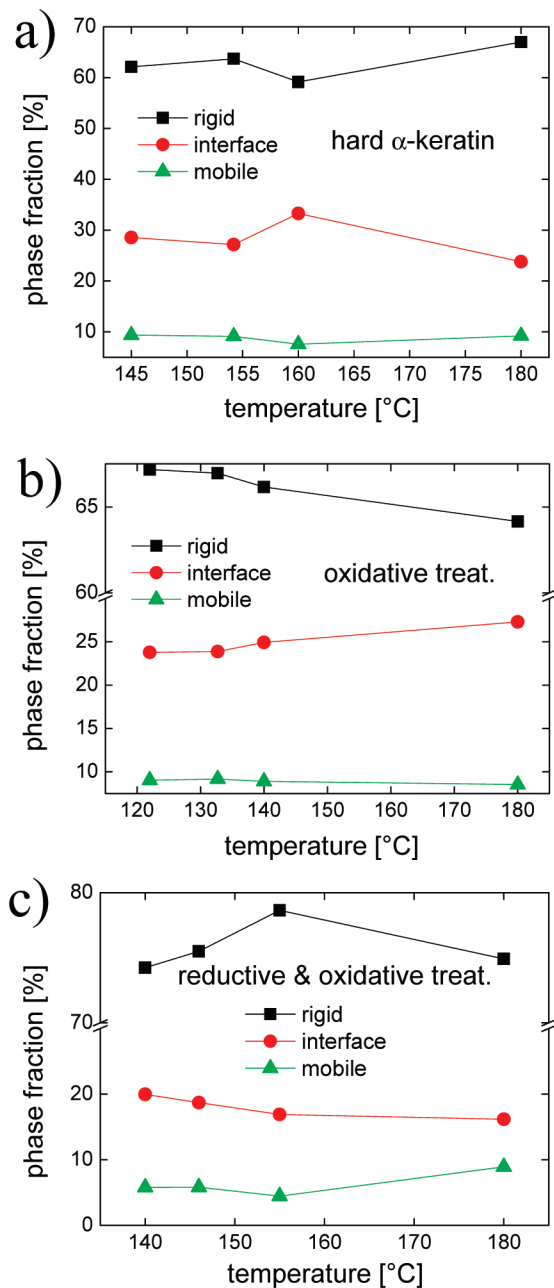


Figure 5. Phase composition of hard α -keratin, in the native state and after oxidative and reductive and oxidative treatments for different temperature ranges.

The DQ filtered NMR spectra recorded for different values of the excitation/reconversion times τ are shown in Figure 7 for the hard α -keratin sample. For short τ values, the DQ filtered ^1H spectrum edits mainly the spin pairs of aminoacids with the strongest dipolar couplings (Figure 7, top). In the region of the maximum of the DQ build-up curves, the pulse sequence edits a dipolar network of many spins corresponding to the crystalline fraction and partially the interface fraction (Figure 7, middle). The ^1H spectrum in Figure 7 (bottom) filtered only the mobile keratin from the amorphous fraction. The value of $\tau = 5 \mu\text{s}$ has been chosen for the dipolar filter of the rigid domain, which still keeps the filter efficiency close to unity with a reasonable value of the signal-to-noise ratio.

4.4. Proton Spin Diffusivities. An accurate analysis of the domain thickness by NMR spin diffusion experiments requires three steps. These are as follows: (i) an optimization of a dipolar filter to obtain the highest selectivity to the different phases,

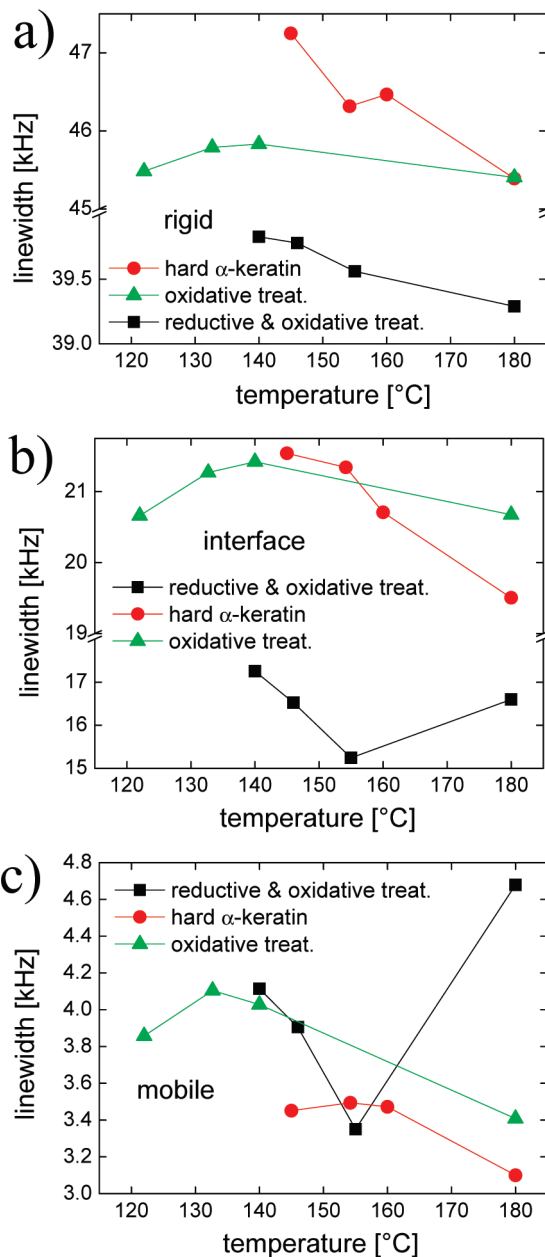


Figure 6. Full line width at half-intensity of the NMR spectral components corresponding to rigid, interface, and amorphous fractions of hard α -keratin, in the native state and after oxidative and reductive/oxidative treatments for different temperature intervals.

(ii) knowledge of the spin diffusion coefficients for modeling the experimental data, and (iii) proper choice of a model that describes the morphology of the material studied.

The values of the spin diffusion coefficients D_R and D_M for the rigid and mobile fractions, respectively, can be determined by approximating the NMR line shapes of the rigid and mobile fractions by Gaussian and Lorentzian functions, respectively. The equations describing the spin diffusion coefficients for the rigid (Gaussian line) and mobile (Lorentzian line) regions are given by²⁰

$$D_R = \frac{1}{12} \sqrt{\frac{\pi}{2 \ln 2}} \langle r^2 \rangle \Delta \nu_{1/2} \quad (12)$$

and

$$D_M = \frac{1}{6} \langle r^2 \rangle [\alpha \Delta \nu_{1/2}]^{1/2} \quad (13)$$

where α is the cutoff parameter of the Lorentzian line, $\Delta \nu_{1/2}$ is the full line width at half-height, and $\langle r^2 \rangle$ is the mean square distance between the nearest spins. An estimation of $\langle r^2 \rangle^{1/2} \approx 0.22$ nm was given for keratin taking into account the amino acid composition.¹³

The calculated spin diffusion coefficients using eqs 12 and 13 are shown in Figure 8. For each denaturation temperature and type of sample, the specific values of D_R and D_M are used for domain size evaluation. The largest value for D_R showing the highest organization and packing corresponds to hard α -keratin (Figure 8a). The morphology deorganization due to reductive/oxidative treatment leads to a reduction of D_R . This trend is also valid for D_M (Figure 8b).

4.5. Morphology and Domain Sizes. The spin diffusion experiments were performed on native hard α -keratin and chemically treated samples after they were heated at the temperatures shown in Figure 3. Proton wide-line NMR spectra recorded at three different diffusion times t_d are shown in Figure 9. In all cases, the flow of magnetization from the rigid domain into the mobile domain is observed with increasing diffusion times. At short diffusion times, mainly the rigid fraction of keratin composed of the α -helical conformation of the intermediate filament is observed, and can be seen in Figure 9 for $t_d = 40 \mu\text{s}$. Upon increasing the spin diffusion time, for example, at $t_d = 250 \mu\text{s}$ and $t_d = 600 \text{ ms}$, the relative intensity of the rigid fraction in the spectra decreases, and the intensity of the narrow line that originates from the soft amorphous fraction represented by the keratin matrix surrounding the intermediate filament increases (Figure 9).

The presence of the highly mobile amorphous regions complicates the interpretation of the spin diffusion data. Due to the fact that it is less than 10% for all samples and that the flow of magnetization is reaching it only after longer spin diffusion times, our approach will mainly focus on the transfer of magnetization between the crystalline and the less-mobile amorphous regions. Therefore, a renormalization of the integral intensities corresponding to these two phases was made by adding the signal of the amorphous phase to the signal of the interface. The time evolution of NMR observables for the reductive and oxidative treated hard α -keratin sample with increasing spin diffusion time is shown in Figure 10 for the rigid and less-rigid fractions. The quasi-equilibrium is reached after about 4 ms, which is less than the longitudinal relaxation times.

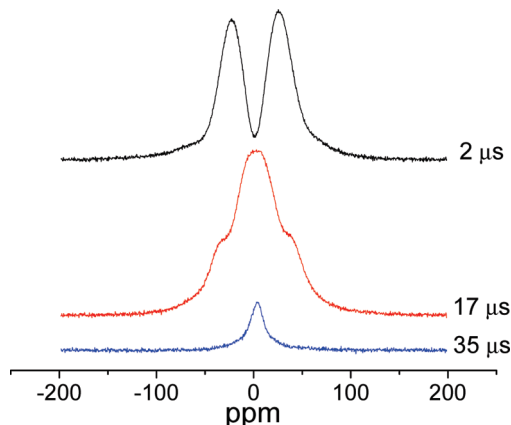


Figure 7. Proton DQ filtered NMR spectra recorded for hard α -keratin at different values of the excitation/reconversion times $\tau = 2 \mu\text{s}$ (top), $\tau = 17 \mu\text{s}$ (middle), and $\tau = 35 \mu\text{s}$ (bottom).

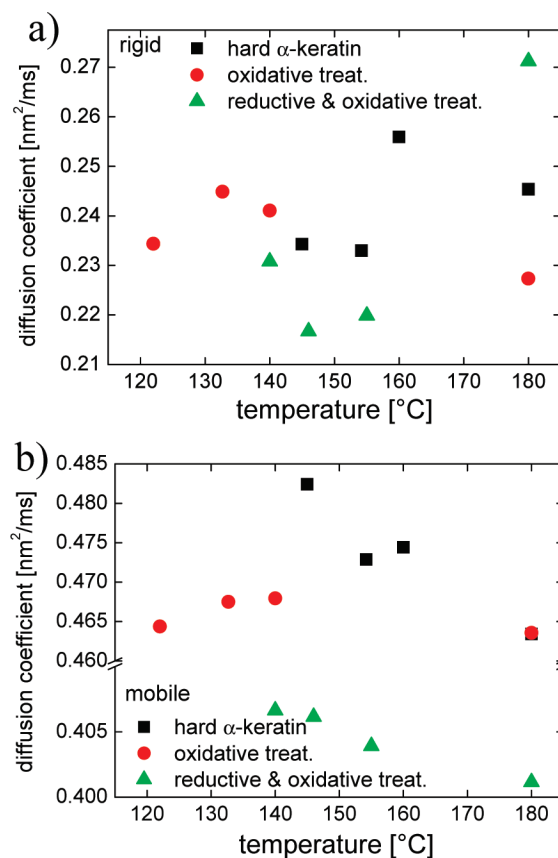


Figure 8. Effective ^1H spin diffusivities D_R (a) and D_M (b) evaluated from eqs 12 and 13 for different hard α -keratin as a function of the denaturation temperature.

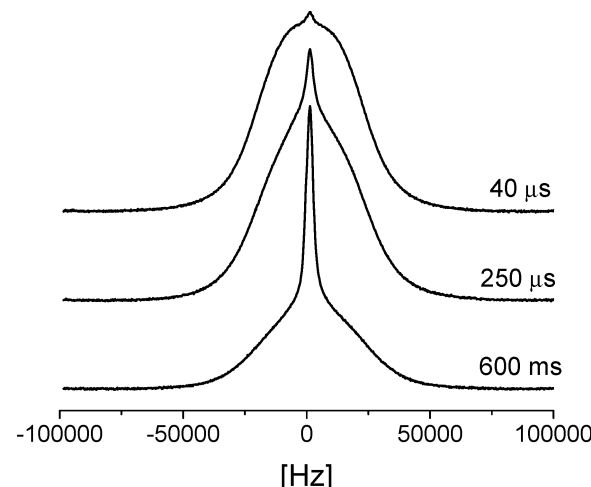


Figure 9. Proton wide-line NMR spectra recorded at three different spin diffusion times t_d of $40 \mu\text{s}$, $250 \mu\text{s}$, and 600 ms after the action of the DQ dipolar filter (Figure 1).

To estimate the domain sizes for the rigid and less-mobile amorphous domains based on the analysis of spin diffusion data using initial rate approximation (section 3.2). The symmetric display of $(t_{d0})^{1/2}$ is shown in the inset of Figure 10, and the two-dimensional (2D) morphology ($\varepsilon = 2$) is considered in eq 10. The values of $(t_{d0})^{1/2}$ for hard α -keratin, in the native state, after oxidative and after reductive and oxidative treatments of the denaturation temperatures are given in Figure 11.

The rigid domain thicknesses of hard α -keratin samples for different denaturation temperatures are presented in Figure 12. It is evident that in the case of reductive and oxidative treatment

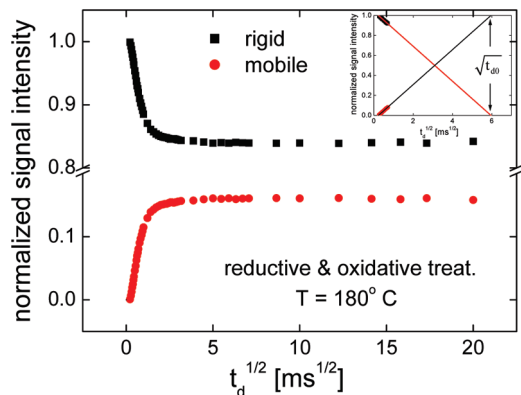


Figure 10. Normalized signal intensities for the ^1H spin diffusion experiment (Figure 1) for a hard α -keratin after the reductive/oxidative treatment and denatured at 180°C . The initial slope and the intercept at $(t_{d0})^{1/2}$ are shown in the inset.

of hard α -keratin the rigid domains do not change in the limit of experimental errors with the denaturation temperatures. Moreover, the disorganization in the intermediate filaments will reduce with about 50% the domain size as compared to hard α -keratin and the sample submitted to the oxidative treatment. For the last two samples, d_R decreases for the largest denaturation temperature.

4.6. Dynamic Heterogeneity of the Hard α -Keratin Fiber Interface. The ^1H spin diffusion experiment using a DQ filter was discussed above for the hard α -keratin at different denaturation temperatures. The evolution of the z -magnetization front can be measured from the spectral component decomposition. At the beginning of the spin diffusion experiment after the action of the dipolar filter, the magnetization is stored only in the rigid domain. For short spin diffusion times, the magnetization is present only in the interface and at the longer diffusion times it will reach the mobile region. The average distance $\langle z^2 \rangle^{1/2}$ traveled by the ^1H z -magnetization can be estimated using the Einstein relationship in one dimension, i.e.,

$$\langle z^2 \rangle^{1/2} \propto \sqrt{2 \left(\frac{D_R + D_M}{2} \right) t_d} \quad (14)$$

where $(D_R + D_M)/2$ is the average spin diffusivity and t_d is the spin diffusion time. Therefore, in the initial time approximation, $\langle z^2 \rangle^{1/2}$ is proportional with $(t_d)^{1/2}$ and also with the average spin diffusivity.

The interfacial region has a gradient in molecular mobility, and therefore, a change in the line width at half-intensity of the spectral component can be detected. At smaller spin diffusion times, the experiment edits the part of the interface closer to the rigid region and at the longer diffusion times the most mobile part of the interface connected to the mobile region. The changes in the line width at half-intensity $\Delta\nu_{1/2}$ of the interface spectral component are shown in Figure 13 for hard α -keratin at different temperatures before and after a denaturation temperature of 154°C . It is interesting that the dynamic heterogeneity of the interface shows a maximum in the molecular mobility. This is more pronounced for the hard α -keratin denatured at $T = 154^\circ\text{C}$. The width of the molecular mobility heterogeneity measured in units of spin diffusion time is almost the same for different temperatures around the DSC denaturation peak (Figure 3). Moreover, the heterogeneity of the molecular dynamics at the interfacial region in hard α -keratin at the extreme temperatures of 145 and 180°C before and after the DSC peak is almost the

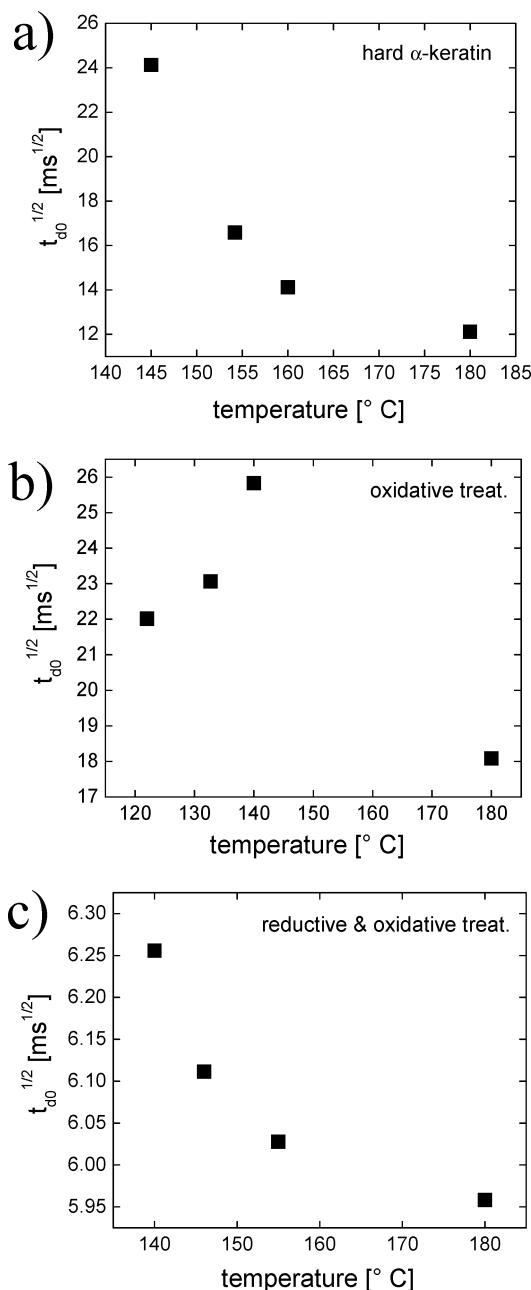


Figure 11. Denaturation temperature dependence of the intercept $(t_{d0})^{1/2}$ for hard α -keratin, in the native state and after oxidative and reductive/oxidative treatments.

same, showing a reorganization of the morphology after the denaturation occurs. Nevertheless, this is not complete because the molecular dynamics at 180°C is slightly faster compared to that at 145°C , as is evident from the right-hand side of Figure 13.

4.7. ^{13}C CPMAS Spectra of Chemically Treated Hard α -Keratin. Cross-polarization (CP) MAS ^{13}C spectra of hard α -keratin, in the native state and after oxidative, reductive/oxidative, and disulfide bond scission treatments at room temperature are shown in Figures 14 and 15. These spectra are similar to those reported for α -keratin of equine hoof under hydrated conditions and thermally denatured wool keratin.^{19,30} Many spinning sidebands are present in these spectra due to the large values of the ^{13}C chemical shielding anisotropy (cf. Figure 14). The ^{13}C CPMAS spectrum of hard α -keratin at a rotor frequency of 5 kHz is shown in Figure 14 where the spinning sidebands are marked by stars.

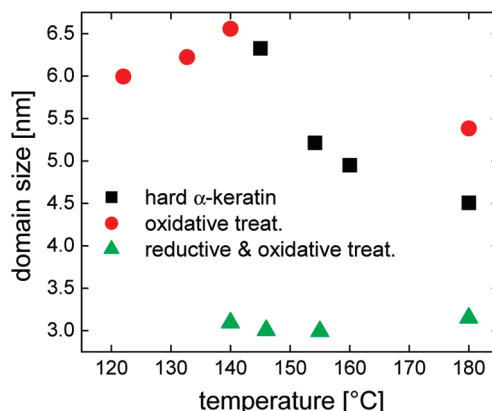


Figure 12. Rigid domain sizes for rigid and mobile + interface fractions of hard α -keratin with different treatments as a function of denaturation temperature.

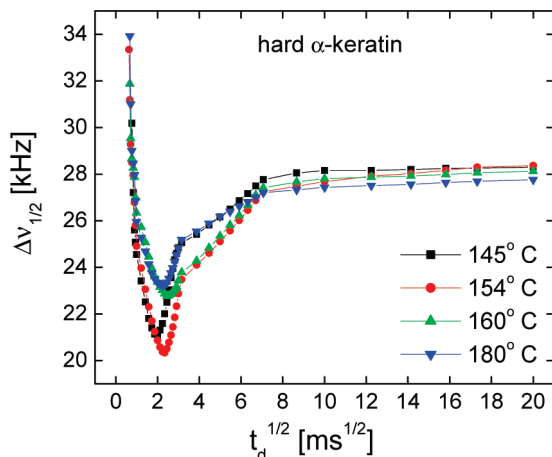


Figure 13. Full line width at half-intensity of the interfacial component of the ^1H NMR spectrum for hard α -keratin measured at different denaturation temperatures.

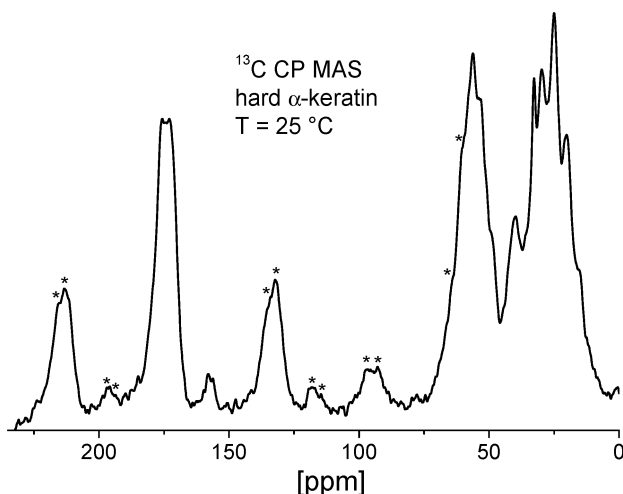


Figure 14. ^{13}C CPMAS spectrum of hard α -keratin at a rotor frequency of 5 kHz where the spinning sidebands are marked by stars.

The ^{13}C spectra show several distinct regions: (i) a broader signal due to the α -carbons at 54 ppm, (ii) the peak at 40 ppm which has contributions from β -carbon in leucine residues and the β -carbon in cross-linked cystine residues, (iii) a complex line shape in the 10–35 ppm region due to alkyl components of the side chains (Figure 15a), and (iv) a carbonyl region with a maximum at 173 ppm (Figure 15b). The assignment was made

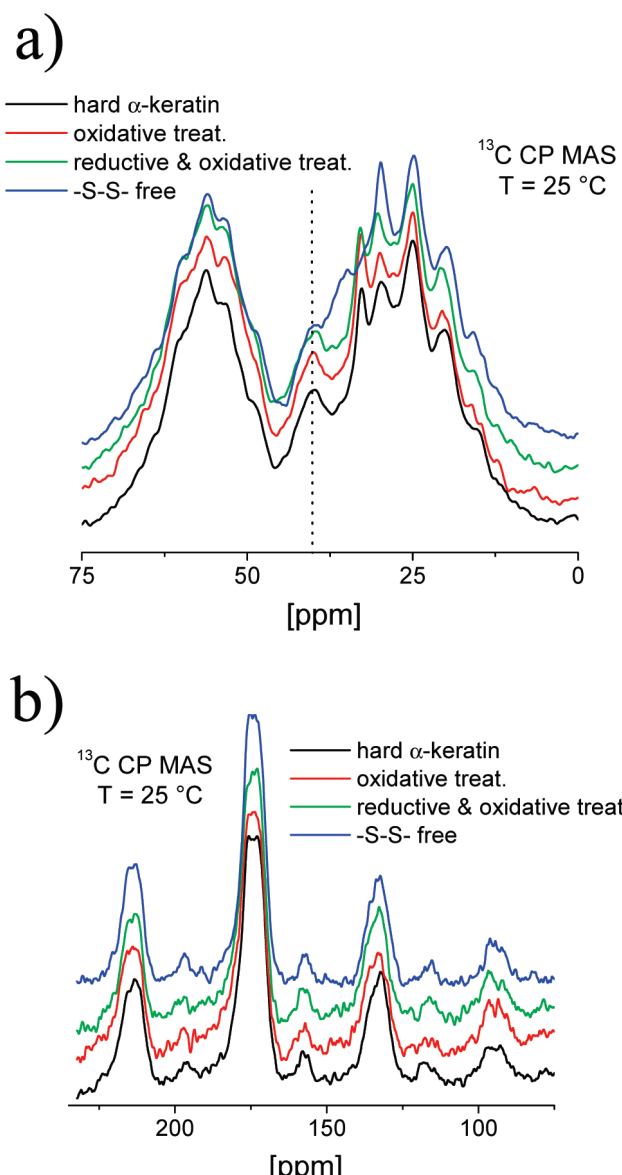


Figure 15. Enlarged version of the alkyl (a) and α -carbon (b) regions of the ^{13}C CPMAS spectra at a rotor frequency of 5 kHz for hard α -keratin, in the native state and after oxidative and reductive/oxidative treatments. The dashed line at 40 ppm marks the ^{13}C resonance of the cysteine engaged in the disulfide links. The ^{13}C CPMAS spectrum of the $-\text{S}-\text{S}-$ bond free sample is also shown.

following the ^{13}C isotropic chemical shifts for the common amino acid residues as reported in ref 19.

In Figure 15a is a zoom of the alkyl and α -carbon regions. The α -carbon shows an increase of intensity, expressed by the shoulder at around 64 ppm, noticeable for the hard α -keratin subjected to oxidative treatment. The peak at 40 ppm is related to β -carbon in cross-linked cystine residues. These participate to the $-\text{S}-\text{S}-$ (disulfide) bonds between neighboring keratin molecules. The intermolecular disulfide links between cysteine residues confer some degree of rigidity to the intermediate filaments in the amorphous matrix component of α -keratin. The intensity and the broadening of the resonance at 40 ppm ^{13}C resonance does not change significantly with the chemical treatment with the exception of the sample where the sulfur of the broken S–S bond was acetylated for arresting its reactivity. This sample has a lower intensity of ^{13}C resonance at 40 ppm compared to the other samples. Moreover, resulting reduced

cysteine residues would be expected to have a β -carbon resonance between 25 and 29 ppm that is indeed revealed in Figure 15a.

The ^{13}C CPMAS spectra from Figure 15b show that the line shape of the carbonyl signal has not changed significantly with chemical treatments. This indicates that the amino acid chains (the keratin molecules) are not significantly damaged (hydrolyzed) by our treatments. A larger degree of disorder of the intermediate filaments would lead to a broadening of the resonances. This disorder will induce ^{13}C chemical shielding tensors with different orientations of the principal reference frames relative to the laboratory frame, leading finally to the line broadening. The broadening of the ^{13}C carbonyl resonance would suggest a shift in the conformation of the α -helix components. For the investigated chemical treatments, the amino acid residue composition does not change, and therefore, the lack of the changing in the carbonyl line shape shows basically the same conformation of the hard α -keratin. This does not stand for the case of hard α -keratin with acetylated sulfur where the line width of the carbonyl signal is slightly larger than the others, suggesting that the acetylation of sulfur after breaking the disulfide bond induced a certain degree of disorder in the hard α -keratin. This supports our view of a three-phase model for the hard α -keratins, where the interface, mainly cystine based, scaffolds the intermediate filaments. The breaking of the cystine and the arresting of the reactive formed thiols by acetylation fragments the scaffold and deprives the intermediate filaments of their mechanical support.

4.8. Thermally Polarized and Laser Hyperpolarized ^{129}Xe Spectra of Chemically Treated Hard α -Keratin. The ^{129}Xe spectra of thermally polarized xenon at room temperature and $p = 20$ bar for hard α -keratin, in the native state and after oxidative and reductive and oxidative treatments are shown in Figure 16a. The sharp weak signal at 40 ppm is a spectrometer artifact. The base of the free gas resonance set as a reference at 0 ppm shows an asymmetry. This distribution of the ^{129}Xe chemical shift in the range 0–15 ppm reflects most probably the xenon atoms trapped between the hair fibers and the defects and the scales at the surface of the fibers. This effect is even better shown by the ^{129}Xe spectra measured using laser hyperpolarized xenon (Figure 16b). The hydrophobic xenon atoms do not penetrate the hard α -keratin and oxidative treated fibers because no ^{129}Xe resonance is detected at larger values of chemical shift. This is not the case for the reductive and oxidative treated fibers where a weak, relatively broad resonance is present in the range 175–190 ppm. We could interpret this resonance as being due to the ^{129}Xe atoms trapped in the voids of the amorphous keratin. The reductive/oxidative treatment produced hydrophobic voids in the keratin amorphous matrix during breaking (reduction) and reformation (oxidation) of the disulfide bonds. The size of these voids can be estimated using the chemical shift (δ_s) of ^{129}Xe atoms originating from the collisions between xenon atoms and the wall of the cavity. This is given by the relationship^{37,38}

$$\delta_s = \frac{49.912}{0.5d_{\text{pore}} - 0.0145} \text{ ppm} \quad (15)$$

valid for low xenon pressure. For the chemical shift around 180 ppm (Figure 16a) from the above equation, we yield $d_{\text{pore}} \approx 0.6$ nm larger than 0.44 nm, the diameter of the xenon atoms. The same result is obtained from the calibration curve presented in ref 39. The size, which is a little bit larger than the usual bonds (disulfide, ionic, hydrogen bonds) between chains in

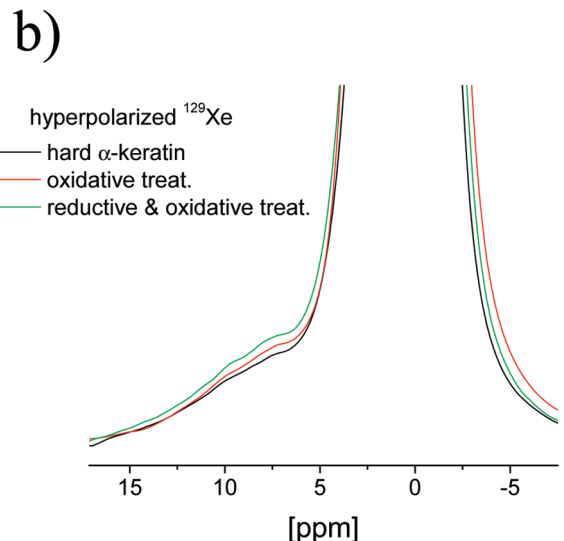
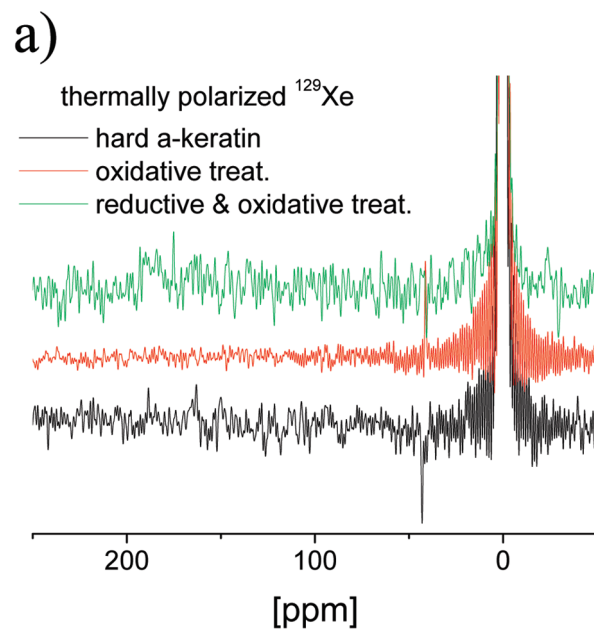


Figure 16. Thermally polarized (a) and laser hyperpolarized (b) ^{129}Xe NMR spectra for hard α -keratin, in the native state and after oxidative and reductive/oxidative treatments.

keratin, is also small enough to speculate that the voids formed from washing out protein material are from medulla. Therefore, we believe that the voids appeared as the result of the incomplete reformation of the disulfide bonds which allowed the chains to arrange less compact than before.

The experiments with laser hyperpolarized ^{129}Xe do not allow us to investigate the bulk of the hard α -keratin and the effects of the chemical treatments due to the loss of the xenon atom polarization induced by the interaction with the matrix. As we already mentioned before, an asymmetric NMR resonance is detected with a good signal-to-noise ratio. The hyperpolarized ^{129}Xe atoms could be confined between the fibers and between the scales of the fiber surface. The distribution of the chemical shift and its small values that is almost the same for all hard α -keratin samples favors the detection of the xenon atoms trapped by the keratin fiber surface.

4.9. Morphological Changes Induced by Chemical and Thermal Treatments as Seen by DSC and NMR Data. The model in Figure 2a gives a simplified schema of a microfibril with protofibrils showing the α -helical rods and the nonhelical

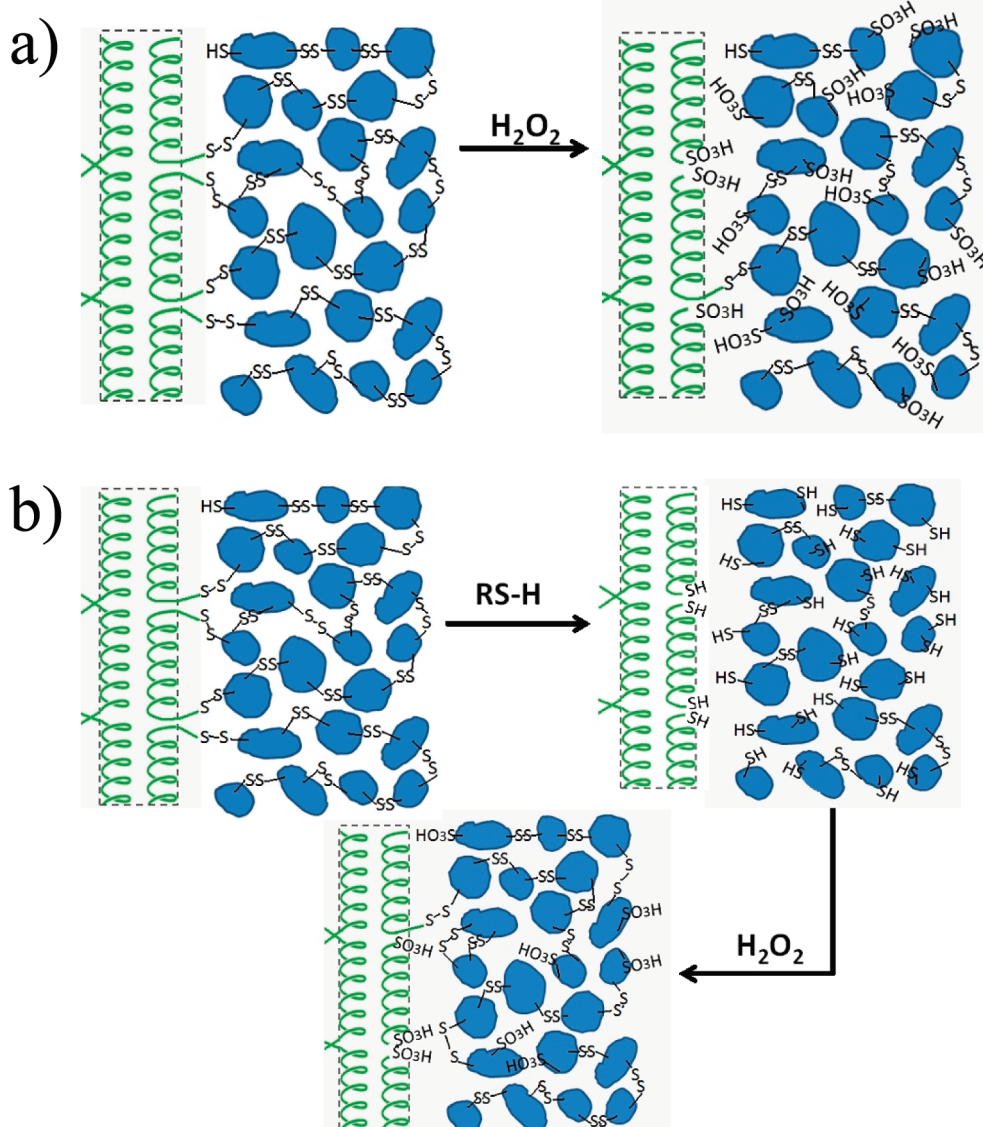


Figure 17. Schematic representation of the intermediate filament (α -helices) imbedded in the keratin amorphous matrix (gray islands). The chemical changes were induced by the oxidative (a) and reductive/oxidative (b) treatments (see text). RSH is the abbreviation for thioglycolic acid.

terminal domains projecting into the interfilamentous space and linking with the matrix proteins through disulfide bonds. The terminal domains contain, besides cystine, glycine, threonine, valine, alanine, and serine, acidic sites such as glutamic and aspartic acid. This scaffolding structure at the IF surface made by the side-chain interactions that anchor the microfibrils to the matrix (interface phase) assists the thermal stability and the primary control over the denaturation of the helical structure of keratin materials when heated. It has a protective role and the capacity to participate in the formation of a solid interface.

The mechanism of thermal denaturation of keratins, as it has been described ref 36 follows several steps. Beyond a certain temperature (the peak on DSC), the temperature rise leads to the breaking of the scaffold structure of IFs. At that temperature, the IFs are in a metastable state. The α -helix denatures at around 80 °C in soluble proteins, and it is only the interface that still keeps it organized. Once set free, the IFs (α -helices) denature. This involves a transition from a relatively compact ordered structure to a more flexible, disorganized, opened polypeptide chain. As the process of denaturation proceeds, the protein molecules unfold and the intern hydrophobic regions expose to the outside of the molecules. The hydrophobic groups in water tend to cluster, leading to associations of molecules.

The chemical modifications we used for the keratin material were focused on attacking the disulfide bonds. The oxidative modification aims at breaking the S–S bonds and oxidizing them into cysteic acid (see Figure 17a). Under the reaction conditions, not all of the bonds will be broken, but overall, it is expected that both the scaffold and the matrix are crumbled. As a result, the DSC peak corresponding to the denaturation of protein shifts toward lower temperature (around 130 °C, see Figure 3) and the enthalpy decreases compared to the original keratin material. The interface amount for oxidative modification is reduced as compared to the hard α -keratin, as shown in Figure 5a and b. Moreover, the molecular dynamics of side chains are intermediate between that of hard α -keratin and the sample subjected to the reductive and oxidative treatment (cf. Figure 6). The rigid domain thickness is not essentially affected by the oxidative treatment (Figure 12).

The reductive/oxidative modification occurs in two steps. First, the S–S bonds are broken by the action of the reductive reagent, thioglycolic acid (TGA), and then are reformed by the oxidative reagent (see Figure 17b). During this sequence of reactions, not all of the bonds are broken and not all of the broken bonds reform; besides, not all of the reformations occur at the same places. In other words, we expect to reform the

material but with a more hindered molecular mobility of the interface and matrix, as shown in Figure 6 obtained from ^1H NMR spectra deconvolution. The rigid fraction increases slightly compared with hard α -keratin (Figure 5a and c), but a reorganization process takes place that reduces the rigid domain sizes (Figure 12). Consequently, the DSC peak is recorded at a temperature between those of not-treated and of oxidative-treated material and has also an intermediary value of the enthalpy (Figure 3).

5. Conclusions

Proton, ^{13}C , and ^{129}Xe NMR spectroscopy and ^1H spin diffusion were used for characterization of phase composition, dynamics of amino acid side chains, domain sizes, the presence of voids at the fiber surface, and in the bulk for hard α -keratin under various chemical treatments and in a range of temperatures including the temperature of denaturation. Proton NMR spin diffusion offers quantitative information about the side chain mobility heterogeneity of the interfacial region. The side chain motions play a very important role in the mechanical deformation of keratin.

These reported NMR results support the thermal denaturation pathway described above according to which concomitantly with the collapse of the scaffolds the α -helices go from a relatively compact ordered structure to a more flexible, disorganized, open polypeptide chain. This is shown by an increase of the mobile phase at the expense of the rigid phase and the interphase. Next, the protein molecules unfold and the intern hydrophobic regions are exposed to the outside of the molecules. The hydrophobic groups tend to cluster in the deuterated water, leading to associations of molecules and rebuilding the amount of the rigid phase from the mobile phase. The interphase amount remains, however, at the same value, as no other reorganization occurs.

Acknowledgment. Support of this project by the Deutsche Forschungsgemeinschaft (DE 780/3-1 and PO 1333/1-1) is gratefully acknowledged. The cooperation with Prof. Stephan Appelt on the hyperpolarized xenon experiments is also acknowledged.

References and Notes

- (1) Popescu, C.; Höcker, H. *Chem. Soc. Rev.*, **2007**, *36*, 1282 and references therein.
- (2) Er Rafic, M.; Doucet, J.; Briki, F. *Biophys. J.*, **2004**, *86*, 3893.
- (3) Parry, D. A. D.; R.D.B. Fraser, R. D. B. *Int. J. Biol. Macromol.* **1985**, *7*, 203.
- (4) Steinert, P. M.; Torkia, D. R.; Mack, J. W. In *Formation and Structure of Human Hair*; Roger, G. E., Reis, P. J., Ward, K. A., Eds.; Chapman & Hall: London, 1989; pp 157–167.
- (5) Parry, D. A. D. *Adv. Protein Chem.* **2005**, *70*, 113.
- (6) Powles, B. C.; Rogers, G. E. In *Formation and Structure of Human Hair*; Jolles, P., Zahn, H., Höcker, H., Eds.; Birkhäuser Verlag: Basel, Switzerland, 1997; pp 59–167.
- (7) Birbeck, M. S. C.; Mercer, E. H. *J. Biophys. Biochem. Cytol.* **1957**, *3*, 203.
- (8) Wortmann, F.-J.; Popescu, C.; Sendelbach, G. *Biopolymers* **2007**, *83*, 630.
- (9) Wortmann, F.-J.; Popescu, C.; Sendelbach, G. *Biopolymers* **2008**, *89*, 600.
- (10) Miles, C.; Ghelashvili, M. *Biophys. J.* **1999**, *76*, 3243.
- (11) Haly, A. R.; Snaith, J. W. *Text. Res. J.* **1967**, *37*, 898.
- (12) Leroy, M.; Cao, J. *Biopolymer* **2005**, *77*, 38.
- (13) Budrugeac, P.; Miu, L.; Bocu, V.; Wortmann, F.-J.; Popescu, C. *J. Therm. Anal. Calorim.* **2003**, *72*, 1057.
- (14) Budrugeac, P.; Miu, L.; Bocu, V.; Wortmann, F.-J.; Popescu, C. *J. Therm. Anal. Calorim.* **2004**, *77*, 975.
- (15) Popescu, C.; Budrugeac, P.; Wortmann, F.-J.; Miu, L.; Demco, D. E.; Baia, M. *Polym. Degrad. Stab.* **2008**, *93*, 976.
- (16) Ernst, R. R.; Bodenhausen, G.; Wokaun, A. *Principles of Nuclear Magnetic Resonance in One and Two Dimensions*; Oxford Univ. Press: Oxford, U.K., 1990.
- (17) Wüthrich, K. *NMR of Proteins and Nucleic Acids*; John Wiley & Sons, Inc.: New York, 1986.
- (18) Duer, M. J., Ed. *Solid-State NMR: Theory and Applications*; Blackwell Science Ltd.: Oxford, U.K., 2001.
- (19) Duer, M. J.; McDougal, N.; Murray, R. C. *Phys. Chem. Chem. Phys.* **2003**, *5*, 2894.
- (20) Mack, J. W.; Torchia, D. A.; Steinert, P. M. *Biochemistry* **1988**, *27*, 5418.
- (21) Perich, J. W.; Johns, R. B.; Thompson, A. R. *Aust. J. Chem.* **1995**, *48*, 1925.
- (22) Yoshimizu, H.; Ando, I. *Macromolecules* **1990**, *23*, 2908.
- (23) Nishikawa, N.; Horiguchi, Y.; Asakura, T.; Ando, I. *Polymer* **1999**, *40*, 2139.
- (24) Nishikawa, N.; Tanizawa, Y.; Tanaka, S.; Horiguchi, Y.; Asakura, T. *Polymer* **1998**, *39*, 3835.
- (25) Schmidt-Rohr, K.; Spiess, H. W. *Multidimensional Solid-State NMR and Polymers*; Academic Press: London, 1994.
- (26) VanderHart, D. L.; McFadden, G. B. *Solid State Nucl. Magn. Reson.* **1996**, *7*, 45.
- (27) Demco, D. E.; Johansson, A.; Tegenfeldt, J. *Solid State Nucl. Magn. Reson.* **1995**, *4*, 13.
- (28) Buda, A.; Demco, D. E.; Bertmer, M.; Blümich, B.; Litvinov, V. M.; Penning, J.-P. *J. Phys. Chem. B* **2003**, *107*, 5357.
- (29) Buda, A.; Demco, D. E.; Bertmer, M.; Blümich, B.; Litvinov, V. M.; Penning, J.-P. *ChemPhysChem* **2004**, *5*, 876.
- (30) Baia, M.; Demco, D. E.; Popescu, C.; Fechete, R.; Melian, C.; Blümich, B.; Möller, M. *J. Phys. Chem. B* **2009**, *113*, 2184.
- (31) Wang, J. *J. Chem. Phys.* **1996**, *104*, 4850.
- (32) Buda, A.; Demco, D. E.; Bertmer, M.; Blümich, B.; Reining, B.; Keul, H.; Höcker, H. *Solid State Nucl. Magn. Reson.* **2003**, *24*, 39.
- (33) Crank, J. *The Mathematics of Diffusion*; Clarendon Press: Oxford, U.K., 1975.
- (34) Goldman, M.; Shen, L. *Phys. Rev.* **1966**, *144*, 321.
- (35) Clauss, J.; Schmidt-Rohr, K.; Spiess, H. W. *Acta Polym.* **1993**, *44*, 1.
- (36) Istrate, D.; Popescu, C.; Möller, M. *Macromol. Biosci.*, DOI: 10.1002/mabi.200800344.
- (37) Ito, T.; Fraissard, J. *J. Chem. Phys.* **1982**, *76*, 5225.
- (38) Demarquay, J.; Fraissard, J. *Chem. Phys. Lett.* **1987**, *136*, 314.
- (39) Ripmeester, J. A.; Ratcliffe, C. I.; Tse, J. S. *J. Chem. Soc., Faraday Trans.* **1988**, *84*, 3731.

JP904484R